X-ray reflectivity study of layering transitions and the internal multilayer structure of films of three-block organosiloxane amphiphilic smectic liquid crystals at the air-water interface

M. Ibn-Elhaj,* H. Riegler, and H. Möhwald

Max-Planck-Institut für Kolloid- und Grenzflächenforschung, Rudower Chaussee 5, D-12489 Berlin, Germany

M. Schwendler

Institut für Physikalische Chemie, Johannes Gutenberg-Universität Mainz, Jacob-Welder-Weg 11, D-55099 Mainz, Germany

C. A. Helm

Fachrichtung Strukturforschung, Universität des Saarlandes, Postfach 1150, D-66041 Saarbrücken, Germany

The structure and layering transitions of ultrathin films of the 4-(5-pentamethyldisiloxypentoxy), 4'-cyanobiphenyl smectic liquid crystal ($5AB$) at the air-water interface has been studied by x-ray reflectivity. By adjusting the molecular area in a Langmuir trough the reversible, layer-by-layer growth starting from a single monolayer was controlled and analyzed. The films consist of a monolayer in direct contact with the aqueous subphase and bilayers on top of it. The thickness of the monolayer ($\cong 12$ Å) suggests a molecular tilt of about 58°. The bilayers are about 36 Å thick, which is approximately the thickness of the bulk smectic A_d phase. Hence, the molecules are presumably in the same interdigitated arrangement of the aromatic cores as in the bulk. A careful analysis of the reflectivity data further indicates a slightly different molecular ordering in the successive bilayers. The interfacial contrast was optionally enhanced, via salt addition, in order to increase the information content and the reliability of the analysis. In these cases ion depletion layers between the bulk subphase and the film were detected. The aromatic parts of the monolayer are found to be partially immersed in water. The bilayer structure itself is not influenced significantly by the addition of ions. [S1063-651X(97)12507-7]

PACS number(s): 64.70.Md, 68.65.+g, 61.10.Kw

I. INTRODUCTION

The influence of the interactions between a surface and an adjacent liquid-crystalline monolayer or multilayer film is of great interest from a fundamental research as well as from a technological point of view [1]. The molecular ordering and orientation within the bulk can be induced by the surface through the anchoring of the molecules at the interface, which depends on the nature of the substrate and the interfaces of the film [2]. This effect is of major importance in the construction of liquid crystal display devices. Although a large research effort has been directed to the design of alignment surfaces that are able to control the molecular orientation, the molecular mechanism of bulk phase anchoring to a surface is still not well understood. This is mainly due to the poor reproducibility and nonuniformity of the alignment, because typically the substrate surfaces are not well defined [1].

It is highly desirable to use a smooth unstructured substrate with a defined and reproducible variability of the chemical potential. This can be achieved by preparing liquid crystals as insoluble monolayers and multilayers at the air-water interface. A strategy for this is to use smectic liquid crystals with polar groups which weakly anchor them at the water surface. By film compression multilayers with discrete layer numbers can be formed successively. With fine tuning of interfacial interactions (e.g., via variation of the substrate

salt concentration) detailed structural studies and interesting comparisons with bulk systems are possible, which then enables the determination of the influence of the air-film interface and water-film interface, respectively, on the film structure.
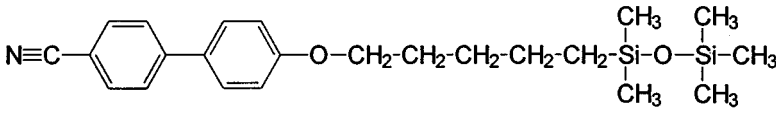
Previous studies on pressure-induced layering transitions have used molecules with weakly hydrophilic groups [3,4] and alkylated liquid crystal molecules. Multilayers have also been observed and investigated using molecules containing cyano groups [5–9]. For these compounds thermodynamics and reversibility were difficult to control since the bulk material tended to crystallize. The smectic liquid crystal 4'-n-octyl-4-cyanobiphenyl (8CB) has been most intensively studied by using surface balance measurements, ellipsometry and optical second-harmonic generation (SHG) [5,6], Brewster angle microscopy [7,8], and surface potential measurements [9]. Yet for 8CB crystallization also occurs for films containing more than three layers [6].

Recently [10] we studied, with film balance measurements and Brewster angle microscopy, the surface pressure induced layering transition of three-block amphiphilic smectic liquid crystals at the air-water interface. SHG and surface potential measurements on films of these smectic liquid crystals are currently being performed and will soon be published [11]. Compared to all others studied, hitherto, these smectic liquid crystals are better suited for the study of layering transitions due to reversibility and a remarkable film stability.

Whereas many x-ray reflection studies on smectic layering on solid substrates and free standing films of liquid crystals can be found in the literature [12–19], so far no x-ray

---

*Author for correspondence. Electronic address: elhaj@mpikg.fta.berlin.de

TABLE I. Molecular structure of $5AB$. Electron number and density of the aromatic, paraffinic, and siloxane parts. The lower value of ρ_{si} is estimated using the density of hexamethyldisiloxane ($d = 0.764$ g/cm^3 [Aldrich catalog]) which is in a liquid state, and the higher one using the additivity of the molar volume of the different molecular parts in the smectic state (data from Ref. [20]).

Molecular structure of 5AB	N≡C—⟨benzene⟩—⟨benzene⟩—O—CH$_2$-CH$_2$-CH$_2$-CH$_2$-CH$_2$-Si—O—Si—CH$_3$ (with CH$_3$ groups)		
Electron number and densities of the molecular parts	$N_e = 101$ $\rho_a \cong 0.40$ e/Å^3	$N_e = 40$ $\rho_p \cong 0.30$ e/Å^3	$N_e = 81$ $\rho_{si} \cong 0.26\text{–}0.30$ e/Å^3
Molecular volume, total electron number, and the average electron density of 5AB	$V_{5AB} \cong 690$ Å^3 $N_{e,M} = 222$ and $\langle \rho_{5AB} \rangle \cong 0.32$ e/Å^3		

reflection studies have been published where the layering transition could be induced by varying the lateral density of a water-insoluble liquid crystal. A particularly interesting question is the propagation of layer ordering perpendicular to the layer normal. In the following we present data from x-ray reflectivity investigations on the successive multilayer formation and details about the internal structure of films of these smectic liquid crystals at the air-water interface.

It will be shown that x-ray reflection provides a sensitive measurement of the electron density perpendicular to the layers, including information on different interfaces. Large Q values up to 0.65 Å^{-1} have been attainable, which allowed direct information on the molecular scale. Since the liquid crystal film exhibits an electron density very close to that of water we can increase the information content and the reliability of the analysis by varying the subphase electron density via salt addition. We can show that the structure of the bilayer section of the film is not affected by this type of contrast variation and we derive microscopic information on the successive layers and on the order evolving within the layers.

II. EXPERIMENT AND ANALYSIS

The investigated liquid-crystalline material 5AB (see Table I), with high performance liquid chromatography (HPLC) purity, is in a fluid smectic A_d phase at room temperature and has a smectic-isotropic liquid phase transition at about 50.3 °C [20]. The layer spacing of the bulk material (36.4 Å) is between one ($l = 22.6$ Å) and two molecular lengths. The molecules are arranged within the layers with a partial overlapping with a certain head-to-head association of the molecules through their cyano dipoles [20].

The monolayers were spread from chloroform solutions (1 mM) on pure water and on concentrated salt solutions (3.4M KCl or 4M NaCl). All x-ray reflectivity measurements were performed at 20 °C. The films were stable during the reflectivity measurements which took from 2 to 15 h. A closed He atmosphere was used to avoid water evaporation, pollution, and background scattering. All experiments were repeated at least once with the same or newly prepared monolayers. No significantly differences in the reflectivity

curves were found. The specular x-ray scattering was performed with a homemade θ/θ setup described elsewhere [21] (Mainz x-ray reflectometer, $U = 40$ kV, $I = 55$ mA, and $\lambda = 1.54$ Å; the system acts as a two-circle diffractometer with unusual geometry. Both the x-ray tube and detector are attached to a geniometer, which can be moved vertically by a lifting jack. In this geometry detector and source are rotated in opposite directions with the same angle θ). The data are background corrected.

Specular reflection of x-rays provides information on the electron-density variation (scattering-density-length variation) perpendicular to the surface with Å resolution. For x rays with a wavelength of $\lambda \cong 1.54$ Å, the index of refraction depends only on the electron density ρ and various constants (r_0 is the classical electron radius $= 2.8 \times 10^{-15}$ m)

$$n = 1 - \frac{r_0}{2\pi} \rho \lambda^2. \tag{1}$$

The reflectivity may be seen as the Fresnel reflectivity R_F of an infinitely sharp interface modulated by interference effects from the thin surface layer. The refractive index of layer and substrate is only slightly less ($\approx 10^{-5}$) than 1. Therefore, dynamic effects (i.e., multiple scattering) or beam refraction contribute significantly to the reflectivity R only at small angles of incidence. Above about two critical angles the reflectivity can be described by the kinematic approximation [22,23]

$$\frac{R}{R_F} = \frac{1}{\rho_{sub}^2} \left| \int \rho'(Z) e^{iQ_Z Z} dZ \right|^2, \tag{2}$$

where ρ_{sub} is the electron density of the bulk phase [$\rho_{sub}(\text{water}) \equiv \rho_w = 0.33$ e$^-$/Å^3 and ρ_{sub} (salt aqueous solution) $\equiv \rho_{salt} = 0.38$ e$^-$/Å^3]; $\rho'(Z)$ is the gradient of the electron density along the surface normal. Q_Z is the wave vector transfer normal to the interface. Due to the loss of the phase information in conventional x-ray reflectivity experiments the data analysis is generally based on finding proper electron-density functions whose reflectivity properties retro-

spectively best match the observed reflectivity data. To obtain the optimum interfacial electron-density variations we used two different strategies.

(i) The layer is subdivided into slabs ("box model") [24,25]. Each box is parameterized by a length and an electron density. The transition between adjacent boxes is smoothed. Proper smearing parameters describe this interfacial roughness. The parameters are determined by a least-squares method. Box models are convenient because they can easily be applied to Eq. (2) and individual boxes may be identified with certain structural properties of the layers (e.g., representing aliphatic chains, headgroups, etc.). For more complex electron-density profiles however, many boxes are necessary to suitably describe the experimental data. This necessitates the determination of more adjustable parameters than one can unambiguously deduce from the reflectivity data and various sets of parameters may result in the same electron-density profile within the experimental errors [21,26].

(ii) The electron-density profile is determined with a method which, to some extent, can be considered model independent [27]. From the experimentally observed reflectivity curve the corresponding profile correlation function is estimated via indirect Fourier transformation. For this profile correlation function the matching scattering-length density profile is then derived by square-root deconvolution. Both the correlation function and the density profile are expressed in terms of a linear combination of a set of suitable basis functions [28]. The coefficients of the linear combination are determined by least-squares techniques. The indirect derivation of the scattering-length density via its profile correlation function has some advantages. The number of basis functions, and thus, that of free parameters, can be optimized (minimized) by a smoothness criterion for the correlation function and, in most cases, no *a priori* assumptions on the shape of the electron-density profile have to be made.

Our interpretation of the reflectivity data was considered satisfactory when the scattering density profiles resulting from the two different modeling processes were equivalent.

III. EXPERIMENTAL RESULTS

A. Isotherms

Figure 1 presents the pressure area isotherms on the water surface and on the concentrated aqueous NaCl solution. In both cases one observes pronounced slope changes corresponding to successive multilayer formation [10]. The changes occur at identical molecular areas indicating equal molecular densities in the corresponding multilayers. It is interesting however, that the pressure of the first plateau (starting at M_1) is affected by the nature of the subphase. We believe that this increased plateau pressure in the case of the concentrated salt solution subphase is related to a deficiency of electrolytes in the interfacial region between subphase and layer whose existence will be demonstrated with the x-ray experiments. This deficiency is probably caused by the repulsion of the ions from the surface by electrostatic image forces. More systematic studies and details concerning the effect of salt and also sugar concentration on the liquid crystal substrate interactions will be given and discussed in a separate paper.
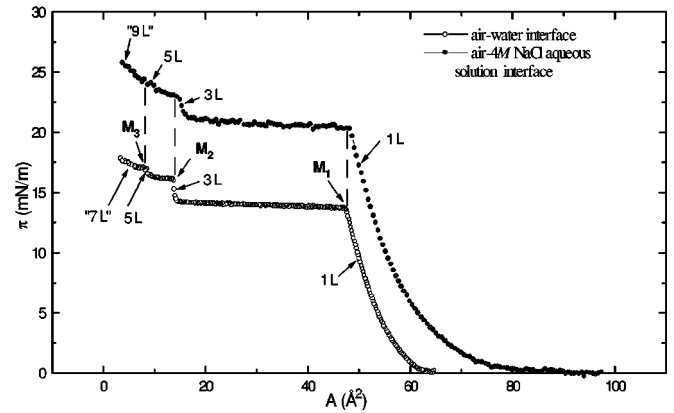

FIG. 1. π-A isotherms at the air-water (open circles) and air-$4M$ NaCl aqueous solution (filled circles) interfaces for 5AB at 20 °C. The sharp breaks of the isotherm slopes, followed by horizontal parts at molecular areas M_1, M_2, and M_3 correspond to successive multilayer formation [see [10] for details]. The arrows indicate points corresponding to x-ray reflectivity measurements (at $A \cong 50 \pm 0.5$ Å^2 for the monolayer, $A \cong 13 \pm 0.5$ Å^2 for three layer ($3L$), $A \cong 7.8 \pm 0.5$ Å^2 for five layer ($5L$), $A \cong 5.2 \pm 0.5$ Å^2 for seven layer ("$7L$"), and $A \cong 4.5 \pm 0.5$ Å^2 for nine layer ("$9L$").

B. X-ray reflectivity of the monolayer

For comparison all reflectivity measurements from monolayers were performed at a fixed area of about 50 Å^2, i.e., at the same packing density in the monolayer on pure water and on the salt solution. With the pure water subphase the monolayer was hardly visible to the x rays. This is probably because the average electron density of the 5AB molecule (0.32 e/Å^3, see Table I) is nearly equal to that of water (0.33 e/Å^3). This problem is alleviated with the concentrated salt solution subphases. In both cases (3.4M KCl or $4M$ NaCl) the subphase electron density is increased to 0.38 e/Å^3. Figure 2(a) shows the x-ray reflectivity curve of the monolayer on the NaCl subphase.

The monolayer thickness can be determined from the minimum in the reflectivity curve [see Fig. 2(a)] to $d_{mo} \cong 12.1 \pm 2.0$ Å according to $Q_{min} = \pi/d$. A careful analysis of the reflectivity data of the monolayer on the salt solution indicated that there is an additional layer between the slab representing the water-free monolayer with d_{mo} and the bulk solution. This probably corresponds to a layer of reduced electrolyte content compared to the bulk electrolyte concentration, which was already mentioned above in the discussion of the plateau pressure shift due to the bulk electrolyte concentration. Indeed, both the model independent and the box model analysis signal this narrow ($\delta = 6 \pm 4$ Å) additional slab of decreased electron density ($\rho = 0.35$ e/Å^3) which corresponds to an electrolyte concentration of $C_\delta \cong 2M$ [see Fig. 2(b)]. The reflectivity data fits are significantly worse without the assumption of the deficiency layer.

The consistency of the fit was checked by comparing the number of electrons per molecule expected from the chemical formula ($N_{e,M} = 222$) with that calculated from the fit parameters. It is found that the number of electrons per molecular area in the top box ($N_e = 190 \pm 50$) agrees reasonably well with that of the entire molecule. Thus it is assumed that the molecules are found predominantly in the top slab. Its
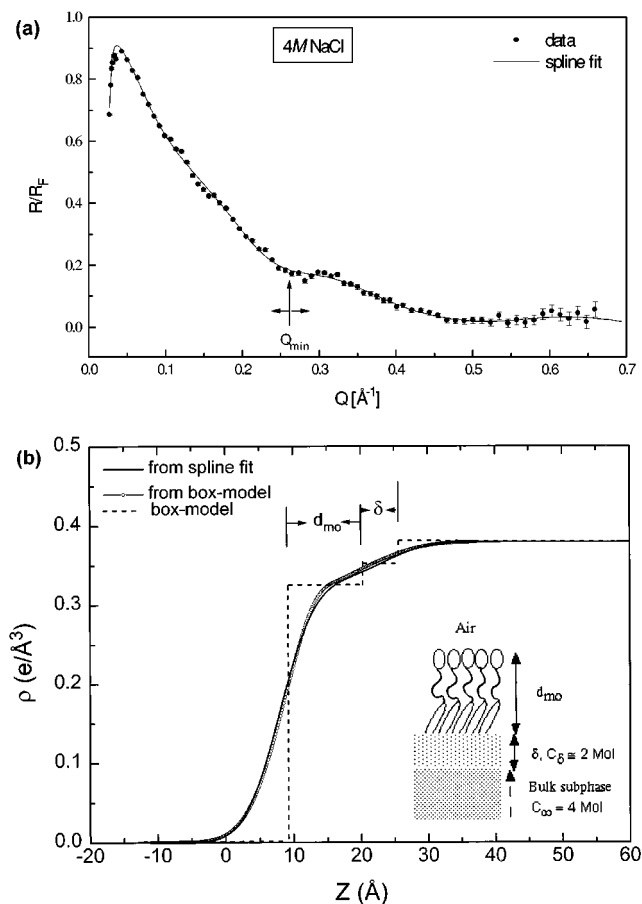
FIG. 2. (a) X-ray reflectivity of the 5AB monolayer on $4M$ NaCl aqueous solution. Circles represent the experimental data. The solid line represents the best spline fit. (b) The corresponding electron-density profile. The inset represents a schematic view of the monolayer on the aqueous salt solution.

FIG. 3. X-ray reflectivity of 5AB multilayers on pure water from $3L$ film (a), $5L$ film (b), and ''$7L$'' film (c). The filled circles represents the experimental data and the opened circles the best spline fits. Solid lines represent the best fits using the box model. The corresponding parameters are listed in Table II.

thickness ($d_{mo} = 12.1 \pm 2.0$ Å) is smaller than the length of a stretched molecule (22.6 Å). This indicates that the molecules are tilted. Assuming a rodlike molecule, we can estimate a tilt angle of $\theta = 58 \pm 7°$ according to $\theta = \arccos$ (12.1/22.6). This tilt agrees with the value determined by SHG ($\theta = 56 \pm 3°$ at 50 Å^2) at the air-water interface [11]. It also matches the value found for monolayers transferred at about 48 Å^2/molecule from the pure water to the silicon substrate (50° Ref. [10]). This supports our earlier assumption that there is no significant change in the tilt angle during the transfer. The same result is obtained for the monolayer on the KCl solution.

C. X-ray reflectivity of multilayers

Figures 3 and 5 show the x-ray reflectivity data for the multilayers (indicated by the arrows in Fig. 1) at the air-water and air-KCl aqueous solution interfaces, respectively. Prior to the following detailed analysis, the obtained curves deserve some general remarks.

(i) For all films one observes a ''Bragg peak'' at $Q \cong 0.15$ Å^{-1} which is related to the smectic layers. As expected the width of the ''Bragg peak'' decreases with the film thickness since the half width at half maximum should be inversely proportional to the square root of the number of layers. This
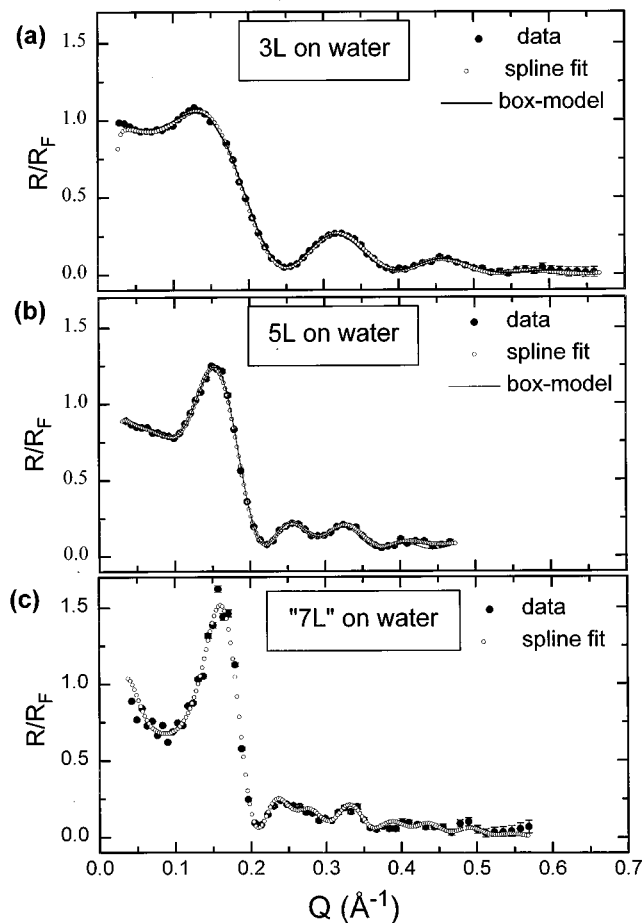
proves the establishment of the smectic ordering upon lateral compression.

(ii) Next to the ''Bragg peak'' a few interference maxima and minima are observed. These ''Kiessig'' fringes are due to the interference at the film-subphase and the film-air interfaces. Their width is roughly inversely proportional to the overall multilayer film thickness. For the $5L$ film the interference pattern is more narrow than for the $3L$ film, indicating an increase of film thickness. As expected, the narrowing of the interference pattern continues for ''$7L$'' and ''$9L$'' films.

Comparison of the $3L$ films (respectively, $5L$ films) on the water and salt solution shows, first, that the minima are shifted to lower Q values with the aqueous salt solutions. This indicates that the films are thicker in the presence of salt. It shows, second, that the position of the Bragg peak is independent of the subphase for the same number of layers which indicates that the structure of the bilayer section of the film is not affected by the addition of salt.

Figure 3 shows the x-ray reflectivity data for the three-layer, five-layer, and ''seven-layer'' films at the air-water interface together with their corresponding fits. The symbol ''$7L$'' means that the film may not be totally homogeneous. This is because the jump of the pressure at the transition
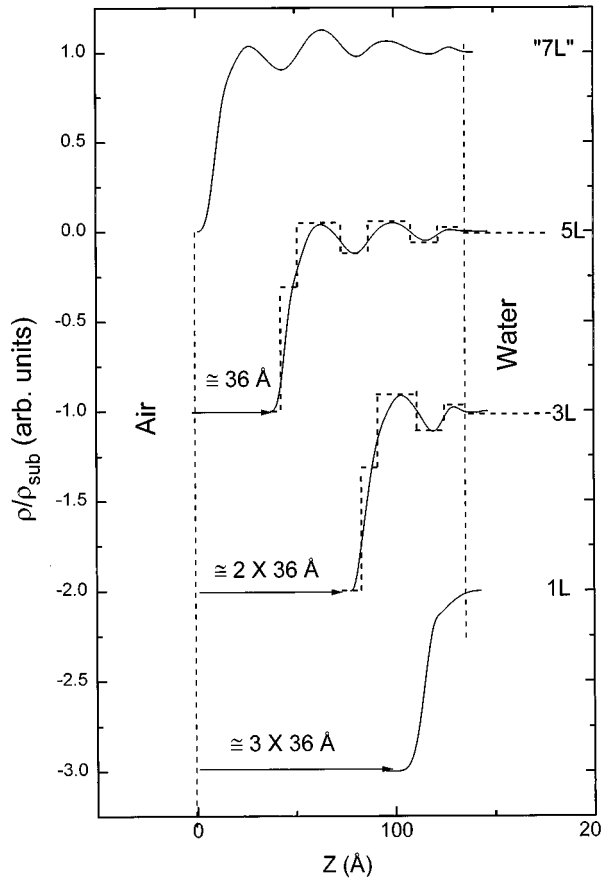
FIG. 4. Electron-density profiles of the monolayer and multilayers derived from the curves in Figs. 2(a) and 3. $1L$ denominates the monolayer on the salt solution. $3L$, $5L$, and "$7L$" label the multilayers on pure water as the subphase. The dashed lines represent the box model without roughness. The curves are shifted by unity along the y axis for a better representation of the layering.

from $5L$ to $7L$ is very small and cannot be resolved experimentally (see Fig. 1). The derived best-fit density profiles (Fig. 4) prove the formation of well-defined, additional layers on top of the monolayer. The average spacing of these additional layers is about 36 Å, nearly equal to that of the bulk smectic A_d phase (36.4 Å) [20]. This confirms our previous conclusion that successive layers are formed upon compression at points M_i [10]. The shapes of electron-density profiles indicate that the films are complete or at least almost complete.

Figure 5 shows the x-ray reflectivity data for $3L$, $5L$, and "$9L$" films at the air-KCl aqueous solution interface with their corresponding fits. The deduced electron-density profiles are shown in Fig. 6. For the upper layers (bilayers) the electron-density profiles on water and on salt solution (see Fig. 7) are quite similar taking into account the experimental error. The electron-density profiles of the films on the electrolyte solution show the additional depletion layer, as already discussed for the monolayers. Both the similarity of the upper layers for different subphases and the additional depletion layer for the salt solution confirm the consistency of our experimental results and data analysis.

All attempts to satisfactorily fit the experimentally measured multilayer reflectivities with simple box models which ignored the intramolecular structure (e.g., considering the $3L$
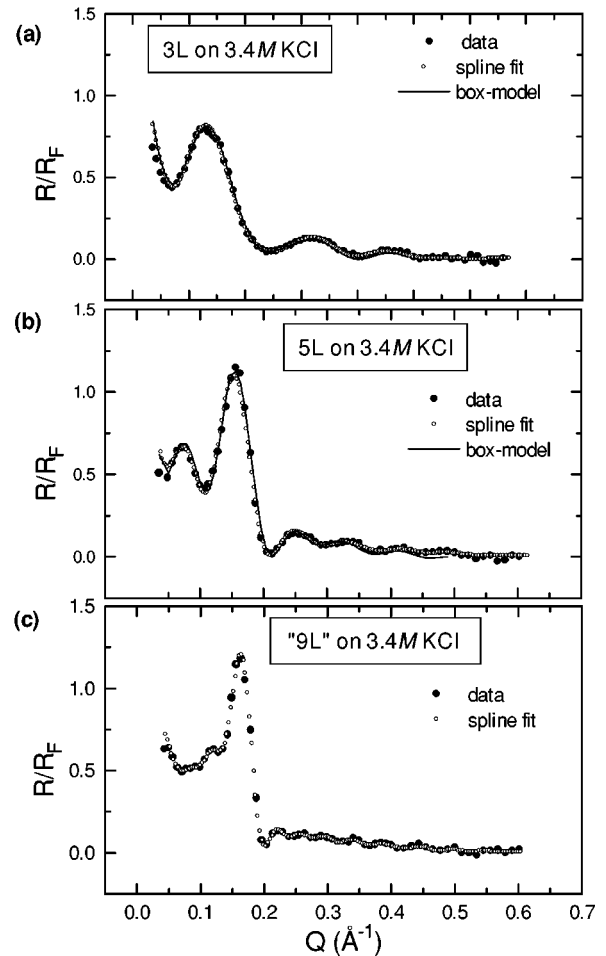

FIG. 5. X-ray reflectivity of 5AB multilayers on 3.4M KCl aqueous solution from $3L$ film (a), $5L$ film (b), and "$9L$" film (c). The filled circles represent the experimental data and the opened circles the best spline fits. Solid lines represent the best fits using the box model. The corresponding parameters are listed in Table II.

film as two boxes describing the first monolayer and the bilayer on top) failed. Therefore, we analyzed the data with box models accounting for details of the internal structure of the multilayer films. We proceeded as follows: The 5AB
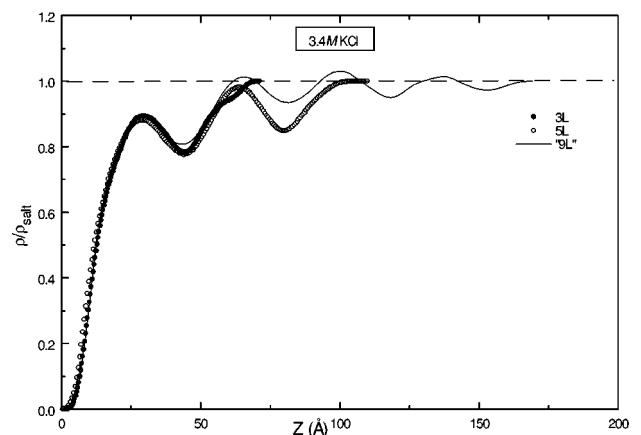

FIG. 6. Electron-density profiles of 5AB multilayers on KCl aqueous solution. The curves are superposed to facilitate comparison (see text).
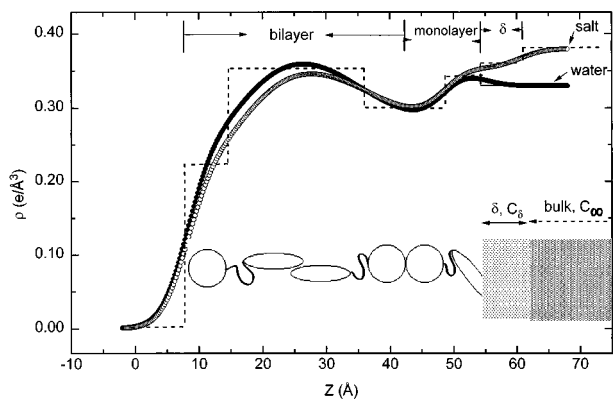
FIG. 7. Comparison of electron-density profiles of $3L$ films on pure water (filled circles) and on aqueous salt solution (open circles). The inset represents a schematic view of the $3L$ film on the aqueous salt solution.
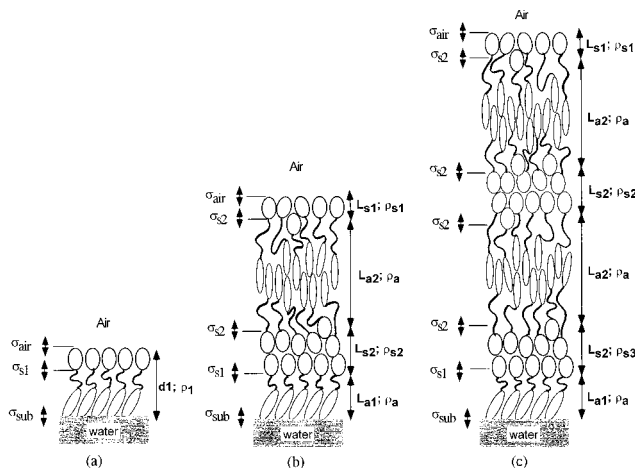

FIG. 8. Schematic representation of the structural model of the film at the air-water interface. (a) monolayer, (b) monolayer plus one overlapped bilayer ($3L$), and (c) monolayer plus two overlapped bilayers ($5L$). Scattering-length densities ρ, sublayer thicknesses L, and roughness σ are defined for each box. The waxy lines represent the disordered paraffin chains, the elongated ellipses represent the aromatic parts, and the nearly circular ellipses represent the siloxane moieties, which are nearly globular in shape.

molecule contains three distinct parts (siloxane, paraffin, and aromatic) which are incompatible with each other. Consequently they tend to segregate into three separate sublayers [20]. Since these parts have different electron densities (see Table I), one might identify each section with its own box. This approach, however, yields a larger number of fit parameters than can reasonably be derived from the experimental data. From the structural model of the bulk smectic layers in the upper layers, bilayering occurs due to the cyano dipole-dipole interaction of the molecules. The bilayer spacing indicates partial overlapping with some head-to-head association which causes a diffuse interface between the aromatic and the paraffin sublayers [20,29]. Therefore it is reasonable to envisage the aromatic and the paraffin parts together as one box and the siloxane part as another separate box. Consequently the three-layer and the five-layer films can be fitted with four-box and six-box models, respectively (see the model with the definition of the box parameters in Fig. 8). All models with a lower number of boxes or a different distribution of the boxes did not describe the experimental data satisfactorily.

It should be noted that in the case of the salt solution the first box adjacent to the subphase does not only contain the paraffinic and the aromatic part of the monolayer, but also the depletion layer of thickness δ. A rigorous analysis would require a separate box for the depletion layer. In a first approach this was, in fact, assumed but it turned out that within the experimental error the electron density ρ_δ is nearly equal to ρ_a. So the two boxes were merged in order to reduce the number of free adjustable parameters.

The number of free-fit parameters could further successfully be decreased by assuming identical sublayer periodicities (box widths) for the siloxane sublayers, L_s, and identical values, L_a, for the aromatic-paraffinic sublayers, respectively. In addition, the electron densities of the aromatic-paraffinic parts ρ_a are assumed to be the same in all boxes. However, it was necessary to assume different electron densities for different siloxane sublayers. Also, fitting with only one roughness failed. Acceptable fits were only obtained when the smearing parameters at the air-film, film-water, and L_{a1}/L_{s2} interfaces (see Fig. 8) are assumed identical ($\sigma_{air} = \sigma_{sub} = \sigma_{s1} \equiv \sigma_1$) and all the other smearing parameters

($\sigma_{s2} \equiv \sigma_2$) for the internal boxes are also identical, respectively. Thus the $3L$ film necessitates 9 fit parameters, the $5L$ film 10. The validity of an approach with so many parameters may be questioned and will be discussed later. The corresponding fits of the $3L$ and $5L$ films on pure water and on salt aqueous solution are also shown in Figs. 3 and 5, respectively.

Our selection of the number and location of the boxes was corroborated by the electron-density profiles based on the spline fits. The fits and resulting density profiles of both fit procedures were equivalent within the measurement errors.

All parameters derived for the different film preparations are listed in Table II. The roughnesses of external and internal interfaces of all films studied are $\sigma_1 = 3-4$ Å and $\sigma_2 = 7-8$ Å, respectively (see Table II). The sublayer spacings agree with the length and expected packing of the molecules (see Sec. IV). Because of the large number of adjustable parameters no attempt is made to fit films thicker than $5L$ with the box model. Nevertheless, since the results were found to be model independent qualitative conclusions can be derived for the thicker films using the electron-density profiles obtained from spline fits.

Within experimental error the fit parameters for the upper boxes are almost the same when the substrate is pure water or salt solution. This is in agreement with the position of the "Bragg peak" which did not change with salt addition. However, the first box in direct contact with the substrate is thicker in the presence of the salt due to the presence of the interfacial electrolyte layer. With a derived average electron density of 0.36 e/Å^3 the electrolyte concentration of the interfacial layer can be determined to $C_\delta \cong 2$ mol, the same value as found for the monolayers.

The hitherto presented results and their validity can be assessed by estimating the number of electrons per unit area from the reflectivity data and comparing it to the values ex-

TABLE II. Scattering-length densities (ρ in e/Å^3), sublayer periodicities (L in Å) and smearing parameters (σ in Å) used in fitting the data of the multilayer films. The parameters are defined in Fig. 8 and $\sigma_{air} = \sigma_{sub} = \sigma_{s1} = \sigma_1$, see text. $N_{e,total}$ is the calculated total number of electrons in the film.

$\rightarrow$ Film $\downarrow$ parameters	Three-layer water	Five-layer water	$\rightarrow$ Film $\downarrow$ parameters	Three-layer KCl
σ_1	3.4 ± 0.4	3.3 ± 0.5	σ_1	3.1 ± 0.5
σ_2	6.4 ± 1.6	5.4 ± 0.9	σ_2	6.2 ± 1.0
ρ_{s_1}	0.22 ± 0.03	0.20 ± 0.03	ρ_{s_1}	0.19 ± 0.03
ρ_{s_2}	0.28 ± 0.02	0.28 ± 0.01	ρ_{s_2}	0.29 ± 0.01
ρ_{s_3}	$\cdots$	0.31 ± 0.01	ρ_{s_3}	$\cdots$
ρ_a	0.37 ± 0.02	0.35 ± 0.01	ρa	0.36 ± 0.01
L_{s1}	6.7 ± 0.5	6.3 ± 0.5	$Ls1$	7.7 ± 0.5
L_{s2}	12.6 ± 1.0	13.7 ± 1.0	$Ls2$	12.5 ± 1.5
L_{a2}	21.4 ± 1.0	22.1 ± 1.0	L_{a2}	20.5 ± 1.5
L_{a1}	4.7 ± 1.5	4.8 ± 1.5	$L_{a1} + \delta$	12.1 ± 1.5
L_{total}	45.4 ± 4.0	82.7 ± 6.0	L_{total}	52.8 ± 5.0
$N_{e,total}$	585 ± 94	1038 ± 116	$N_{e,total}$	688 ± 95

pected from the isotherms and the chemical formula. The average number of electrons can be calculated as follows:

$$N_{e,total} = \sum_{i=1}^{n} N_{e,i} = \sum_{i=1} A_i \rho_i L_i,$$

with $N_{e,i} = A_i \rho_i L_i$ the number of electrons in box i. A_i, ρ_i, and L_i are the corresponding molecular area, electron density, and length. n is the number of boxes used in the fit model.

From the isotherms a molecular area of $A_{mo} = 46$ Å^2 for the monolayer and a molecular area of $A_{bi} = 38$ Å^2 for the upper layers [10] is assumed. Hence, the number of electron sper molecular area in the first box (situated in the monolayer part, see Fig. 8) of the $3L$ film as calculated from the reflectivity data is $N_e = 80 \pm 30$ on pure water and $N_e = 200 \pm 30$ on the aqueous salt solution. Nearly the same values are derived for the first box of the $5L$ film for the respective subphases. The comparison with the expected number of electrons calculated from the chemical formula ($N_e = 141$) indicates that parts of the molecules are immersed in the water ($N_e = 61 \pm 30$ electrons) and thus do not contribute to the x-ray reflectivity. In the presence of salt the large number of electrons is due to the depletion layer which contributes to the thickness of the first box.

Since in the fit procedure some constraints are imposed especially for the internal boxes, it is unreasonable to individually deliberate the number of electrons in each box. Only the total number of electrons may be considered a meaningful parameter. Taking into account the observed partial immersion of the first monolayer, the derived total numbers of electrons (see Table II) are in acceptable agreement with the ones expected from the chemical formula: from the isotherm the ratio of the number of electrons in the bilayer and the monolayer is $N_{e,bi}/N_{e,mo} \cong 2.4$ (see Ref. [10]). Thus the total number of electrons expected from the chemical formula are $N_{e,3L} = N_{e,mo} + N_{e,bi} = 222 + 2.4 \times 222 \cong 755$ for the $3L$ film and $N_{e,5L} = N_{e,mo} + 2N_{e,bi} = (222) + 2.4 \times 2 \times 222 \cong 1288$ for the $5L$ film.

IV. DISCUSSION

The results of this report are based on the analysis of x-ray reflectivity data. The derivation of the electron-density profiles from the reflectivity data is not unambiguous because of the loss of the phase information in x-ray reflectivity. The data are generally analyzed by trial-and-error methods (modeling), i.e., finding a proper set of parameters which together with the related basis functions describe best the observed reflectivity behavior. Due to the complicated reflectivity curves and internal film structure we needed a large number of free parameters to get acceptable fit results. This calls for some general remarks on the fitting procedure and its significance.

(i) The reflectivity curves were fitted by two different methods: the spline function approach, which is to some extent model independent, and the box model method. In all cases both fit procedures yielded virtually the same results.

(ii) The measured reflectivity curves contain many details (e.g., several minima) with only low noise. This enables and vindicates the determination of detailed electron-density profiles with high precision.

(iii) The variation of the substrate electron density corresponding to a contrast variation. Although the subphase electron density is varied by merely 15% the impact on the scattering curves is drastic because the electron densities of all boxes are similar to that of pure water (see, e.g., the structure of the $3L$ reflectivity curves near 0.1 Å^{-1}). Thus up to three independent measurements (i.e., on different subphases) of the same or almost the same film could be obtained and compared. Due to these three facts it is justified to assume that the derived electron densities are significant and reflect the real film structure.

The total film thickness could be determined with good accuracy. This total film thickness as "seen" by the x rays is not necessarily identical with the "real" thickness because of the partial immersion of the aromatic part of the monolayer in water. This immersion and the existence of a salt depletion layer can be derived from a comparison of the results obtained with the subphase contrast variation.

Our data prove that the multilayer films consist of a monolayer and bilayers on top. The monolayer has a thickness of about 12 Å [see Table II and Fig. 2(b)]. This corresponds to an average tilt angle of 58°. The upper bilayers posses an average thickness of about 36 Å, which is approximately the thickness of the bulk smectic A_d phase [20]. This confirms our previous conclusion that successive and complete layers are formed upon compression at points M_1 [10].

In addition to the total film thickness our x-ray reflectivity data provide information about the modulation of the electron density and thus about the internal structure of the film along the substrate normal. Acceptable fits were only obtained when the roughnesses of the internal interfaces between siloxane and paraffin sublayers (σ_{s2}) are larger than those at the top of the film (σ_{air}) and at the paraffin-siloxane interface in the monolayer (σ_{s1}). This may be due to the different areal cross sections of the different molecular parts. Hence, in the bilayer section some siloxane parts should be dissolved in the adjacent paraffin sublayer as it is the case in the bulk smectic phase [20]. In the monolayer part, the molecular areas can accommodate without partial dissolution of the siloxane parts because the aromatic parts are tilted. At the air-film interface the interfacial energy is reducing the roughness.

The comparison of the top bilayers of different films is also interesting. Within experimental error the electron densities of all these bilayers are the same (see, e.g., Fig. 6). This may suggest that the upper bilayers have the same structure, which is probably imposed by the air. Probably the anchoring field strength, at the air-film interface, is dominating over the film-substrate interfacial interactions (see also Refs. [19] and [30]).

Within the same film the top bilayers always have a lower electron density than those underneath. This may indicate some specific order or existence of molecular holes in the top bilayer.

There are also indications (from careful comparison of distances between the minima in the electron-density profiles) that the first bilayer adjacent to the monolayer at the air-water interface is slightly thinner than the bulk smectic period and also than those of the internal bilayers of the thick films (e.g., from careful comparison of distances between the minima in the electron-density profile of ''9L'' film, see Fig. 6). This might indicate a stronger interdigitation, some molecular tilt, or both. The bilayer thinning near the substrate implies an increase of the molecular area (lateral expansion of the bilayer). This could be due to the necessity of the molecular area of the upper layers to match that of the first monolayer in which the molecular area is larger (46 Å^2) than in the bulk (38 Å^2). Transient ordering has been observed in thin films of other liquid crystals [31,32] or Langmuir-Blodgett films [33]. In the present case the bilayer thicknesses seem slightly different. However, the resolution of our reflectivity data is not high enough to unambiguously prove any specific transient molecular ordering. Further detailed investigations are necessary on this topic.

V. SUMMARY AND CONCLUSIONS

We have investigated via x-ray reflectivity monolayers and multilayers of a three-block amphiphilic 4-(5-penta-methyldisiloxypentoxy), 4'-cyanobiphenyl smectic liquid crystal at the air-water interface. The reflectivity data were carefully analyzed with two different model procedures to ensure maximum significance of the obtained electron-density profiles. The results confirm the successive and complete formation of multilayers upon film compression as predicted earlier [10]. The thickness of the first monolayer at the air-water interface suggests that the molecules are tilted at an angle of about 58°. Part of the aromatic section of the monolayer is probably immersed in the water subphase and does not contribute to the monolayer thickness ''seen'' by the x rays because of a negligible electron-density difference between the immersed section and pure water. This could be revealed via contrast variation of the aqueous subphase. By replacing the pure water by concentrated salt solutions the electron density of the subphase was increased significantly. It is found that the bilayer structure is essentially not affected by this change of the subphase. However, in the case of the high salt concentration one observes a salt depleted layer just beneath the monolayer of several Å thickness. This depletion is probably caused by electrostatic image forces and leads to the observed increase of the plateau pressures in the isotherms. The bilayers on top of the monolayer have thicknesses comparable to those of the smectic bulk phase suggesting a similar molecular packing with partial interdigitation (head-to-head association) of the aromatic parts. Careful analysis of electron-density profiles further reveals that the successive bilayers are slightly different. Bilayers adjacent to the monolayers at the film-subphase interface seem to have some transient packing. On the other side, independently from the total number of bilayers, all top bilayers seem to have similar structure probably imposed by the air.

The investigations show that it is possible to reversibly create monolayers and multilayers at the air-water interface with suitable molecules. X-ray reflectivity is an excellent tool to probe the molecular ordering of such films. It is, however, necessary to very carefully analyze the data and to cross-check the significance by other means, for instance by (contrast)variation of the subphase. This latter technique also yields additional insights into the head-group–subphase interactions. To obtain further details on the molecular ordering in general, and especially on the indicated transient ordering, more careful studies, preferentially by other methods like x-ray diffraction, SHG, surface potential measurements, IR spectroscopy, and neutron reflectivity on deteurated compounds seem advisable. Nevertheless, the presented results already show the small, yet significant impact of the different interfaces on the molecular ordering.

[1] See, for example, J. Cognard, *Alignment of Nematic Liquid Crystals and their Mixtures* (Gordon Breach, London, 1982).

[2] B. Jerome, Rep. Prog. Phys. **54**, 391 (1991).

[3] B. Rapp and H. Gruler, Phys. Rev. A **42**, 2215 (1990).

[4] B. Rapp, M. Eberhardt, and H. Gruler, Makromol. Chem. **46**, 439 (1991).

[5] P. Guyot-Sionnest, H. Hsiung, and Y. R. Shen, Phys. Rev. Lett. **57**, 2963 (1986).

[6] J. Xue, C. S. Jung, and M. W. Kim, Phys. Rev. Lett. **69**, 474 (1992).

[7] M. C. Friedenberg, G. G. Fuller, C. W. Frank, and R. Channing, Langmuir **10**, 1251 (1994).

[8] M. N. G. de Mul and J. A. Mann, Langmuir **10**, 2311 (1994).

[9] P. Schmitz and H. Gruler, Europhys. Lett. **29**, 451 (1995).

[10] M. Ibn-Elhaj, H. Riegler, and H. Möhwald, J. Phys. (France) I **6**, 969 (1996).

[11] M. Harke *et al.* (unpublished).

[12] J. L. Janning, Appl. Phys. Lett. **21**, 173 (1972).

[13] J. Als-Nielsen, F. Christensen, and P. S. Pershan, Phys. Rev. Lett. **48**, 1107 (1982).

[14] B. M. Ocko, A. Braslau, J. Als-Nielsen, and M. Deutsch, Phys. Rev. Lett. **57**, 94 (1986).

[15] B. M. Ocko, P. S. Pershan, C. R. Safinya, and L. Y. Chiang, Phys. Rev. A **35**, 1868 (1987).

[16] J. Als-Nielsen, in *Topics in Current Physics*, edited by W. Schommers and P. Blackenhagen (Springer, Berlin, 1987), Vol. 43, p. 181.

[17] E. F. Grambergen and W. H. de Jeu, J. Phys. (France) **49**, 363 (1988).

[18] P. S. Pershan, J. Phys. (France) **50**, C7-1 (1989).

[19] B. M. Ocko, Phys. Rev. Lett. **64**, 2160 (1990).

[20] M. Ibn-Elhaj, H. J. Coles, D. Guillon, and A. J. Skoulios, J. Phys. (France) II **3**, 1807 (1993).

[21] H. Baltes, M. Schwendler, C. A. Helm, and H. J. Möhwald, J. Colloid Interface Sci. **178**, 135 (1996); H. Baltes, Ph. D. thesis, University of Mainz, Germany, 1995.

[22] J. Als-Nielsen, *Structure and Dynamics of Surfaces In Topics in Current Physics*, edited by W. Schommers and P. Blackenhagen (Springer, New York, 1986).

[23] J. Als-Nielsen and H. Möhwald, *Handbook of Synchrotron Radiation*, edited by S. Ebashi, M. Koch, and E. Rubenstein (Elsevier, Amsterdam, 1991), Vol. 4.

[24] C. A. Helm, H. Möhwald, K. Kjaer, and J. Als-Nielsen, Europhys. Lett. **4**, 697 (1987).

[25] L. Bosio, J. J. Benattar, and F. Rieutord, Rev. Phys. Appl. **22**, 775 (1987).

[26] I. M. Tidswell, B. M. Ocko, P. S. Pershan, S. R. Wasserman, G. M. Whitesides, and J. D. Axe, Phys. Rev. B **41**, 1111 (1990).

[27] J. S. Pederson, J. Appl. Crystallogr. **25**, 129 (1992); J. S. Pederson and I. W. Hamley, *ibid.* **27**, 36 (1994).

[28] O. Glatter, J. Appl. Crystallogr. **10**, 415 (1977).

[29] D. Guillon and A. Skoulios, Mol. Cryst. Liq. Cryst. **91**, 341 (1983); J. Phys. (France) **45**, 607 (1984).

[30] E. Smela, and J. Martinez-Miranda, Liq. Cryst. **14**, 1877 (1993); E. Olbrich, O. Marinov, and D. Davidov, Phys. Rev. E **48**, 2713 (1993).

[31] E. F. Grambergen, W. H. de Jeu, and J. Als-Nielsen, J. Phys. (France) **47**, 711 (1986).

[32] Y. Galerne, Europhys. Lett. **18**, 511 (1992).

[33] A. Asmussen and H. Riegler, J. Chem. Phys. **104**, 8159 (1996).